Earthquakes and Structures, *Vol. 15, No. 2 (2018) 179-191*
DOI: https://doi.org/10.12989/eas.2018.15.2.179

Dynamic performance of a composite building structure under seismic ground motions

Meng-Hao Tsai*[1], Junfei Zhang[2a], Yih-Ping Song[1a] and Jun-Kai Lu[1b]

[1]*Department of Civil Engineering, National Pingtung University of Science and Technology, Pingtung 912, Taiwan*
[2]*School of Civil, Environmental and Mining Engineering, The University of Western Australia, Crawley, WA 6009, Australia*

(Received June 5, 2017, Revised May 7, 2018, Accepted May 8, 2018)

Abstract. This study is aimed at investigating the dynamic performance of a composite building structure under seismic ground motions. The building structure is an official fire department building located in southern Taiwan. It is composed of a seven-story reinforced concrete (RC) and an eight-story steel reinforced concrete (SRC) frame. Both frames share a common basement and are separated by expansion joints from the first to the seventh floor. Recorded floor accelerations of the building structure under eight earthquakes occurring during the period from 2011 to 2013 were examined in this paper. It is found that both frames had similar floor acceleration amplifications in the longitudinal direction, while the SRC frame revealed larger response than the RC frame in the transverse direction. Almost invariant and similar fundamental periods under the eight earthquakes in both directions were obtained from their transfer functions. Furthermore, numerical time-history simulations were carried out for the building structure under the most intensive earthquake. It is realized that the seismic response of the composite building was dominated by the first translational mode in each horizontal direction. Higher modes did not significantly contribute to the structural response. The conventional Rayleigh damping model could be appropriately applied to the time-history simulations under bi-directional excitations. Approximate floor acceleration envelopes were obtained with a compound RC and SRC structural model by using the average damping ratios determined from the different structural arrays.

Keywords: composite building structure; seismic performance; floor acceleration; time-history simulation

1. Introduction

Earthquake-induced building collapse can cause hundreds of thousands of deaths. A recent example was the Meinong earthquake, which occurred in Kaohsiung, Taiwan on February 6th, 2016 and resulted in over one-hundred dead. Structural and life safety under severe ground motions has made the observation of seismic response of critical infrastructures an important topic for a long time (Takewaki *et al*. 2013, Sharma *et al*. 2016, Bikçe and Çelik 2016, Ruiz-Pinilla *et al*. 2016, Mihailov *et al*. 2000, Inel and Meral 2016, Isik and Kutanis 2015). Many countries in the earthquake prone regions, such as America, Japan, China, Taiwan, North Korea, Chile, and Mexico, have applied seismic response monitoring technique to important civil structures. For instance, Los Angeles City of America has included instrumentation arrays in high-rise buildings analyzed and designed by using non-linear response history procedures recommended in Chapter 16 of ASCE-7 guidelines (LATBSDC 2011). A detailed history of building instrumentation programs within the United States is available in Celebi (2004). United States Geological Survey (USGS) and California strong Motion Instrumentation Program (GSMIP) have measured seismic responses for over 300 buildings, dozens of dams, bridges, and special structures (Garevski 2013). A number of measurement techniques have been applied to many buildings and bridges in order to estimate their possible damages under earthquakes and typhoons (Ansari 2005). Lemnitzer *et al*. measured aftershock response data of four RC buildings in Santiago, Chile with instrumentation consisting of uni-axial and tri-axial accelerometers as well as some displacement transducers (Lemnitzer *et al*. 2014). Michel *et al*. (2010) applied earthquake recordings, ambient vibrations and modeling for the evaluation of full scale dynamic response of an RC building under weak seismic motions. The measured responses can be used to examine conventional design assumptions for future code modification. Moreover, monitoring techniques have made system identification, model updating (Skolnik *et al*. 2006, Yu *et al*. 2008), damage detection and long-term health monitoring (Bradford *et al*. 2004, Doebling 1996, Celebi *et al*. 2004) possible and resulted in code provisions such as fundamental period formulas (Lemnitzer *et al*. 2014, Goel and Chopra 1998). Data collected from temporarily and permanently instrumented buildings have enabled significant researches on seismic response of building structures. The change of vibration frequencies identified from measured time-history response has been used as an indicator of structural damage (Doebling 1996, Clinton *et al*. 2006, Mucciarelli *et al*. 2004). Numerical modeling has been an efficient approach to simulate dynamic structural responses under ground excitations. The measured seismic

*Corresponding author, Professor
E-mail: mhtsai@mail.npust.edu.tw
[a]Graduate Student
[b]Professor

ISSN: 2092-7614 (Print), 2092-7622 (Online)

Fig. 1 The front view of the fire department building

response can be used to calibrate the structural analysis model and evaluate the validity of some design assumptions (Ventura *et al*. 2003). The structural analysis model can be further used to predict the nonlinear dynamic response under strong earthquakes (Irie *et al*. 2000). It can be confirmed that combination of civil structures and interdisciplinary technology has become the trend of global civil engineering development.

Strong ground motion and structural instrumentation arrays have been developed over decades in Taiwan. Since 1989, 823 free-field ground motion arrays and instrumentation of 58 civil structures have been established island-wide (Shin *et al*. 2002). In the initial stage of establishment, the structural instrumentations were applied to important and special structures located in seismically active and/or metropolitan areas like Taipei, Taichung, Chiayi, Hualien and Taitung. Few structural arrays were constructed for the southern Kaohsiung and Pingtung districts where the seismicity is less active. Nevertheless, for the nationwide establishment of seismic structural arrays and seismic response observation of a representative governmental building in the southernmost county in Taiwan, the Pingtung Fire Department Building was instrumented with thirty-two accelerometers in 2010. Since then, seismic responses of the building under dozens of earthquakes have been collected by the structural arrays. This study is aimed at investigating the seismic performances of the fire department building under several larger earthquakes. Consistency between the original design and real seismic spectra was evaluated with the *in-situ* ground motions. Measured floor accelerations were used to examine the adequacy of the assumed floor amplification factors in the seismic design code. Also, time-history simulations for the seismic response of the building under the most intensive earthquake were carried out. The conventional Rayleigh damping model was appropriately applied to the dynamic simulations for the building structure.

2. Structural overview and instrumentation

2.1 Overview of the building structure

The fire department building, which was built in 2000, is used as the firefighting offices and emergency response centers for Pingtung County, as shown in Fig. 1. From the original design drawing and *in-situ* survey, the building has eight stories from the basement (B1F) to the roof (RF). The

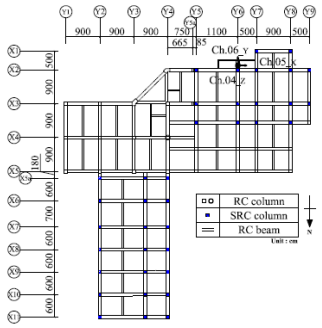

Fig. 2(a) Structural plan of B1F

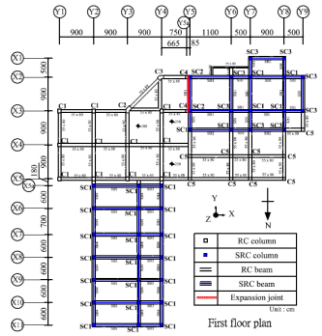

Fig. 2(b) Structural plan of 1F

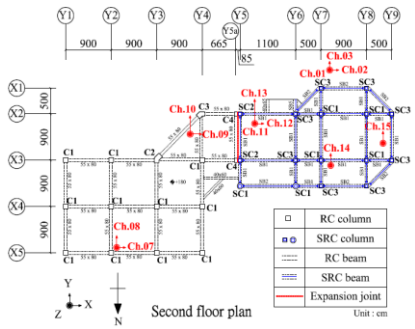

Fig. 2(c) Structural plan of 2F

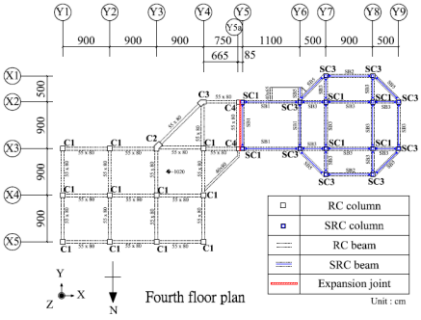

Fig. 2(d) Structural plan of 4F~7F

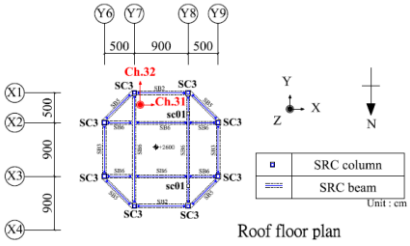

Fig. 2(e) Structural plan of RF

B1F and 1F floors are below the ground level with the lowest elevation of the B1F being -540 cm. Both stories have a consistent floor area with 64.5 m and 70.8 m in projected length and width, respectively, as shown in Figs. 2(a) and 2(b). The B1F is used as parking lots and machine rooms. Elevation of the 1F is -180 cm such that more than half of the first story is below the ground level. However, part of the first story connects to an open space outside of the building. All the other floors above the ground level have an identical floor plan except the 2F and 3F. Both the 2F and 3F have a very similar structural plan as shown in Fig. 2(c). Typical structural plan from the 4F to the 7F is shown in Fig. 2(d). The projected plan dimensions from the 2F to 7F are 64.5 m in length and 32.0 m in width. As indicated in the figures, the building structure is in fact composed of a reinforced concrete (RC) and a steel reinforced concrete (SRC) moment resisting frame above the first floor. They are completely separated by an expansion joint from the 4F to the 7F, as shown in Fig. 2(d). However, their slabs are partially connected at the 1F, 2F, and 3F, as observed in Figs. 2(b) and 2(c). There is a concrete water tank on the 7F of the RC part, which is the top of the RC frame and has an elevation of 2250 cm. However, the top of the SRC frame is a roof protrusion from the 7F and used as the apron of helicopter, as shown in Fig. 2(e). It is defined as the RF of the department building and has an elevation of 2600 cm. Both frames share a common basement with raft foundation.

2.2 Seismic resistant design of the building

According to the seismic design code in 2000 (CPA 1997), the seismic design force of the building, denoted as V, was calculated as

$$V = \frac{ZI}{1.4\alpha_y F_u} CW \tag{1}$$

where Z was the seismic zone factor and equal to 0.23. C was the acceleration spectrum coefficient and W was the building weight. I was an importance factor and equal to 1.5 for the seismic design since the building was categorized as an important building. α_y and F_u were the initial yielding factor and the seismic reduction factor, respectively. Based on the structural height from the 1F to the 7F, the natural period is calculated as 0.77 sec by using the code formula $T = 0.07 h_n^{3/4}$ with h_n=24.3 m. Soil condition of the building site is classified as normal (Type-II Soil) according to the SPT-N values of nearby boring data. Hence, the design acceleration spectrum coefficient C is estimated as 1.79. Considering the ductility capacity provided by moment-resisting frames, the seismic reduction factor F_u is calculated as 2.9. With the code-defined over-strength factor 1.4 and an initial yielding factor 1.5, the equivalent peak ground acceleration (PGA) for elastic seismic design is 0.085. This implies that elastic behavior under ground motions with PGA less than 0.085g was assumed in the structural design. Also, with the design acceleration spectrum coefficient, the seismic coefficient is calculated as 0.10.

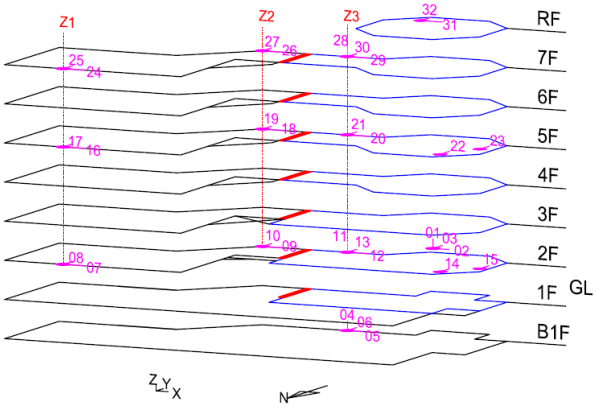

Fig. 3 Deployment of structural arrays

Table 1 Numbering of the accelerometers

Floor	RC frame				SRC frame	
	Z1 axis		Z2 axis		Z3 axis	
	X	Y	X	Y	X	Y
2F	07	08	09	10	12	13
5F	16	17	18	19	20	21
7F	24	25	26	27	29	30

2.3 Layout of the structural arrays

Thirty-two uniaxial accelerometers were installed in the building by the Central Weather Bureau of Taiwan in 2010. The deployment of the instrumentation arrays is shown in Fig. 3. Three orthogonal accelerometers were installed on the B1F and two on the RF. Also, three accelerometers were deployed outside the building for free-field ground motions. The rest ones were distributed on the 2F, 5F, and 7F. For convenience, these accelerometers are categorized by the Cartesian coordinate system with x, y, and z representing the longitudinal, transverse, and vertical direction, respectively, as indicated in Fig. 3. In addition, three vertical axes, namely Z1, Z2 and Z3, are assigned to the structural arrays with similar xy-plane coordinates on the 2F, 5F, and 7F. The corresponding channel numbers and directivity are summarized in Table 1. The Z1 and Z2 axes are located in the RC frame and the Z3 axis in the SRC frame. Measured acceleration time histories on the Z1, Z2, and Z3 axes are used to evaluate the seismic performance of the department building in this study.

3. Seismic performance of the building

3.1 Seismic events

Seismic responses of the fire department building under dozens of earthquakes have been recorded since 2010. However, the maximum structural accelerations under most earthquakes were less than 10 gal. After preliminary screening, eight seismic events with larger structural responses were selected as shown chronologically in Table 2. Fig. 4 shows the epicenter locations of the eight earthquakes. All of them have a Richter magnitude larger

Table 2 Details of the eight earthquakes

No.	Date	Longitude	Latitude	Depth (km)	Richter magnitude (M_L)	Epicenter distance (km)
1	2011/03/16	120.68	22.56	34.9	4.7	24.5
2	2011/03/20	121.38	22.44	27.5	5.8	95.6
3	2012/02/26	120.76	22.75	26.3	6.4	28.0
4	2012/06/06	121.42	22.44	18.4	5.9	99.5
5	2012/06/07	120.58	22.92	15.5	4.5	26.9
6	2012/06/09	122.31	24.46	69.9	6.6	270.2
7	2012/10/25	120.37	22.43	40.7	5.4	31.8
8	2013/06/02	120.97	23.86	14.5	6.5	138.7

Table 3 Horizontal PGA of the eight earthquakes (unit: gal)

No.		1	2	3	4	5	6	7	8
X	B1F	6.82	9.03	41.35	6.04	2.95	2.52	17.79	14.80
	Free field	9.42	9.28	47.34	6.67	3.79	2.78	20.25	15.31
Y	B1F	11.77	11.18	39.47	6.30	2.60	2.69	9.16	12.50
	Free field	16.92	12.02	40.63	6.49	2.82	2.85	11.42	12.51

Table 4 Estimated peak structural roof drift ratios under the eight earthquakes ($\times 10^{-5}$)

No.	1	2	3	4	5	6	7	8
Z1-X	3.81	2.49	8.04	2.16	1.52	1.49	4.22	3.23
Z2-X	3.15	3.01	14.93	2.10	1.37	1.20	4.27	3.01
Z3-X	3.85	4.67	12.09	3.23	1.97	1.15	5.33	3.61
Z1-Y	4.93	4.06	20.67	2.85	2.08	1.84	3.80	4.67
Z2-Y	3.27	3.76	25.11	2.62	2.16	2.27	3.91	5.51
Z3-Y	8.36	8.18	48.27	4.89	2.95	2.75	6.71	9.78

than 4.5 and the largest one is equal to 6.6. The horizontal PGAs recorded at the free field and the B1F are shown in Table 3. It is seen that all the PGAs were less than 0.085g and both the free field and B1F had similar PGAs for most cases. In addition, the peak roof drift ratio has been suggested as a suitable engineering demand parameter for the structure response (Cruz and Miranda 2016). Hence, the 7F and the B1F acceleration records were processed with Butterworth filter and then doubly integrated to calculate the peak structural drift ratios on the Z1, Z2, and Z3 axes, as summarized in Table 4. Since all the peak drift ratios are small, it is inferred that the building behaved elastically under the eight earthquakes.

3.2 Acceleration response spectrum

The first step in the investigation of the seismic records is constructing the acceleration response spectra. They can reveal the basic characteristics of the input ground motions and local site conditions. Figs. 5(a) and 5(b) present the normalized 5%-damped acceleration response spectra obtained from the longitudinal (*X*-axis) and transverse (*Y*-axis) accelerometers at the free field, respectively. The corresponding counterparts obtained at the B1F are shown in Figs. 6(a) and 6(b). It can be seen that the B1F and free field have very similar response spectra. Also, Table 3

Fig. 4 Epicenter locations of the eight earthquakes

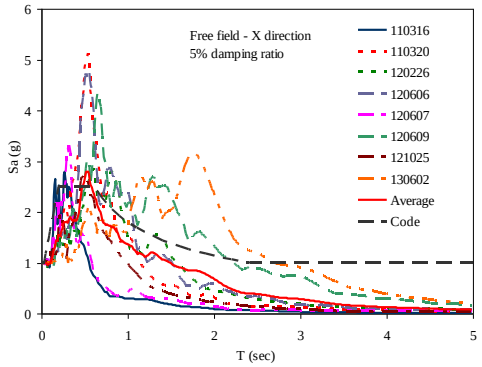

(a) Longitudinal

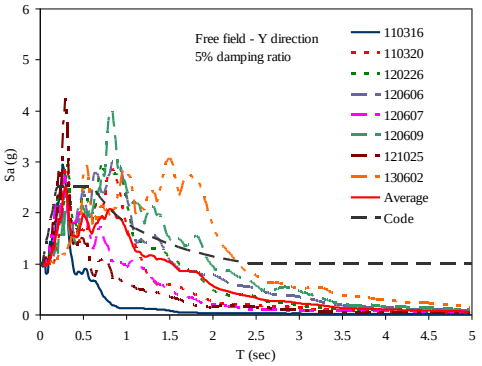

(b) Transverse

Fig. 5 Normalized 5%-damped free-field acceleration response spectra

reveals that both of them have approximate PGAs. This means the local soil condition is of little influence on the wave propagation from the free field to the B1F. The acceleration time histories of the B1F are used as the seismic input in later analysis. In the same figure, the average response spectrum of the eight earthquakes is compared with the 5%-damped seismic design spectrum of the building. It is seen that the design spectrum approximately envelops the average spectrum, which indicates that the former may capture the quake characteristics at the building site.

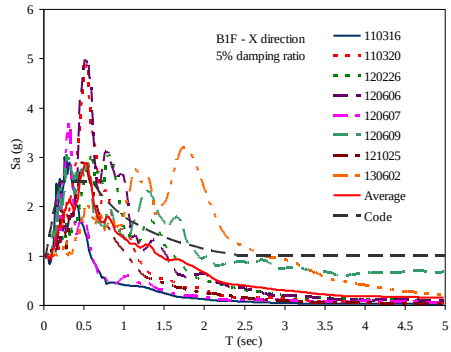

(a) Longitudinal

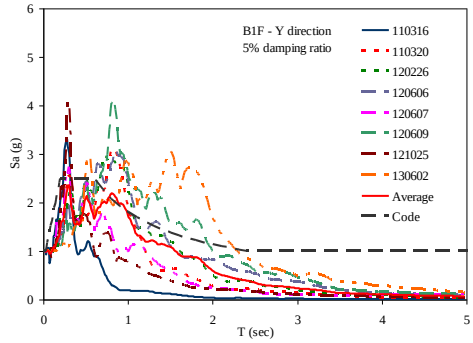

(b) Transverse

Fig. 6(a) Normalized 5%-damped B1F acceleration response spectra

3.3 Floor acceleration response

According to the layout of the structural arrays, the acceleration amplifications of the 2F, 5F, and 7F at the aforementioned Z1, Z2, and Z3 axis are shown in Figs. 7, 8, and 9, respectively. They were calculated by dividing the maximum and minimum floor accelerations by the PGA at the B1F. As observed from the figures, the amplifications of the 2F are approximate to 1.0 in all cases. Since the basement and part of the first story are under the ground level, the RC retaining walls surrounding the B1F and 1F make the stories below the 2F behave like a rigid body. From Figs. 7 and 8, it is observed that the longitudinal (*X*-axis) and transverse (*Y*-axis) amplifications were generally similar. Meanwhile, although the RC frame does not have a perfectly regular structural plan, it seems that the torsional effect is not significant since the floor amplifications on the Z2 axis were only slightly different from that on the Z1 axis. An empirical formula (1+2*z*/*h*), where *z* is the floor height and h is the total structural height from the base, has been recommended in ASCE 7-10 (ASCE 2010) and FEMA-450 (2003) guidelines for estimating the floor acceleration. The current seismic design code of buildings in Taiwan also adopts the empirical formula to determine the seismic design force of attached equipments on different stories. The formula reveals a linear variation of floor acceleration amplification from 1.0 at the base to 3.0 at the roof. The mean response in Figs. 7 and 8 indicate that the empirical formula can serve as a good approximation for the floor acceleration amplification of the RC frame.

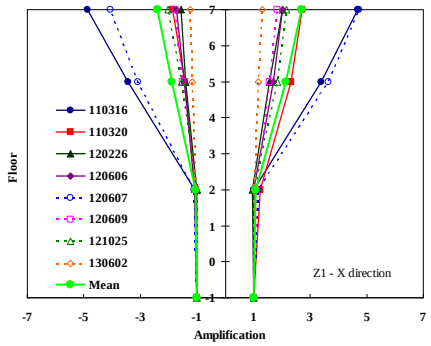

(a) Longitudinal

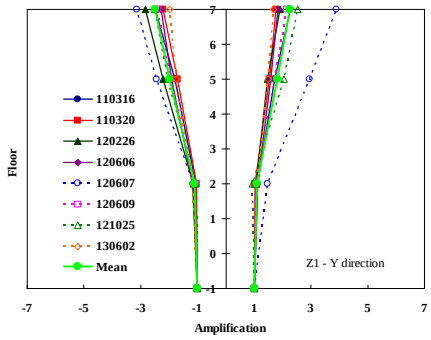

(b) Transverse

Fig. 7 Floor acceleration amplifications at the Z1 axis

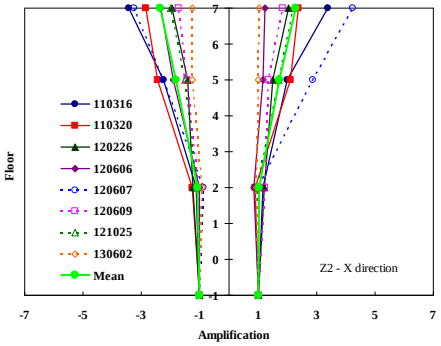

(a) Longitudinal

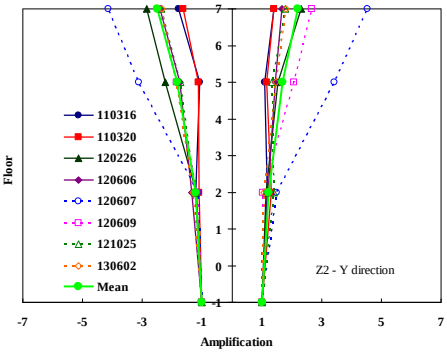

(b) Transverse

Fig. 8 Floor acceleration amplifications at the Z2 axis

Fig. 9(a) shows that the longitudinal acceleration amplifications of the SRC frame were similar to that of the RC frame. However, as shown in Fig. 9(b), the SRC frame had apparently larger acceleration amplifications in the transverse direction. This implies that the RC and SRC

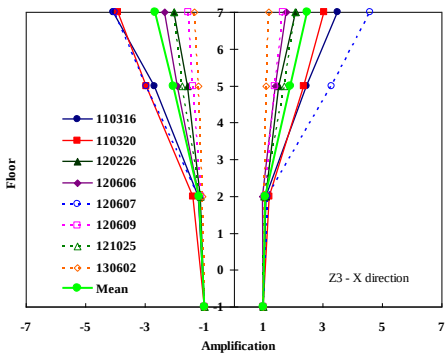

(a) Longitudinal

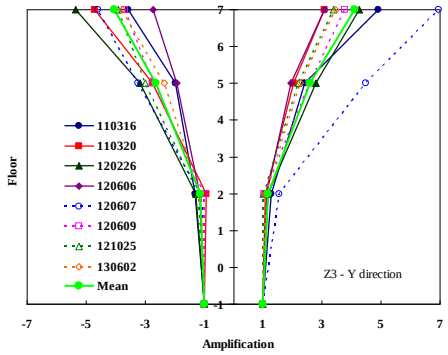

(b) Transverse

Fig. 9 Floor acceleration amplifications at the Z3 axis

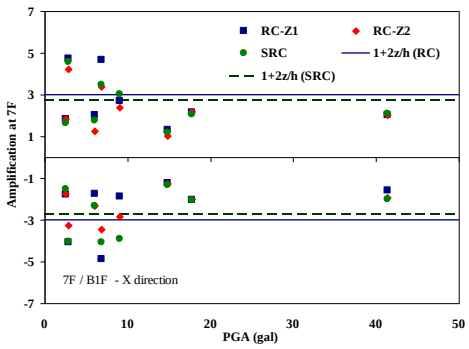

(a) Longitudinal

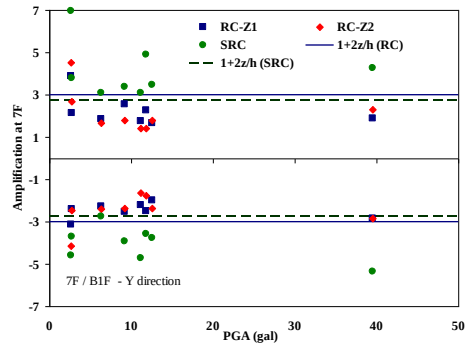

(b) Transverse

Fig. 10 Variation of the 7F acceleration amplification with PGA

frames could have joined seismic behavior in the longitudinal direction, although there is an expansion joint disconnecting both frames. Therefore, the empirical formula of the ASCE 7-10 guideline obviously underestimates the transverse acceleration amplification of the SRC frame. The empirical formula (1+3*z*/*h*), which is recommended in UBC-97 (ICC 1997), seems more appropriate instead.

Figs. 10(a) and 10(b) show the variation of the 7F longitudinal and transverse acceleration amplifications with the PGA, respectively. It can be observed that the acceleration amplification did not show a direct relation with the PGA. This is consistent with the aforementioned empirical formulae for predicting the floor acceleration amplification, which are independent of the PGA. In Fig. 10(a), most of the acceleration amplifications were bounded by the empirical prediction (1+2*z*/*h*), although more scattered variation was induced under ground motions with smaller PGA. However, the same empirical prediction resulted in smaller transverse acceleration amplifications for the SRC frame, as shown in Fig. 10(b).

4. Estimation of fundamental period

Using the measured B1F acceleration as input and the 7F as output, transfer functions of the three designated vertical axes were constructed to estimate the fundamental period of the building structure. Figs. 11, 12, and 13 show the transfer functions under the eight earthquakes at the Z1, Z2 and Z3 axes, respectively. As observed from Figs. 11(a), 12(a), and 13(a), the fundamental period in the longitudinal direction (*X*-axis) was around 0.29 sec (3.5 Hz) for the Z1 axis and 0.33 sec (3.0 Hz) for the Z2 and Z3 axes. It was approximate to 0.42 sec (2.3 Hz) for all the Z1, Z2, and Z3 axes in the transverse direction (*Y*-axis), as observed from

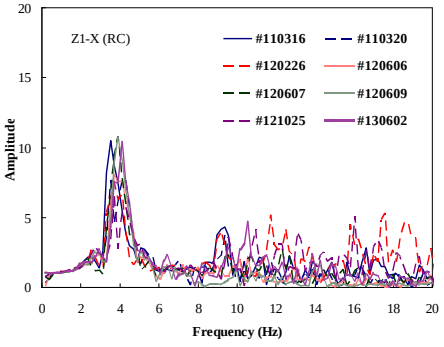

(a) Longitudinal

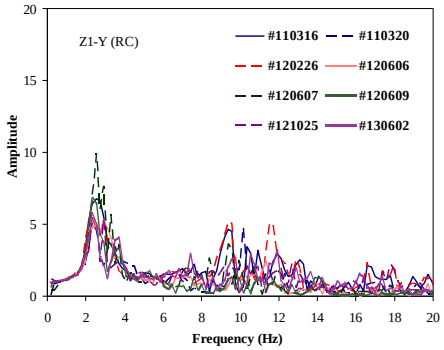

(b) Transverse

Fig. 11 Transfer functions at the Z1 axis

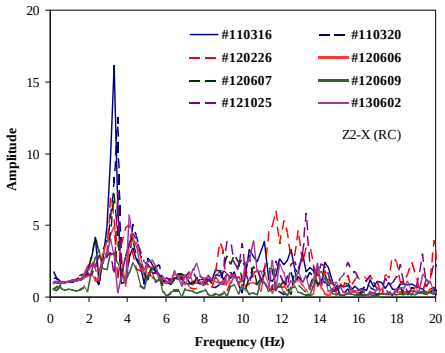

(a) Longitudinal

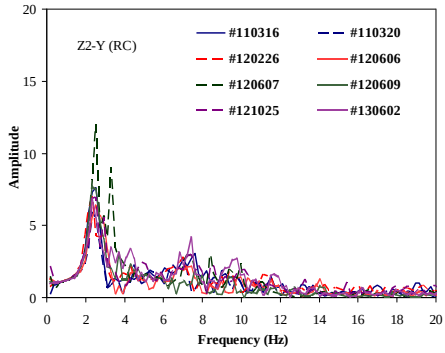

(b) Transverse

Fig. 12 Transfer functions at the Z2 axis

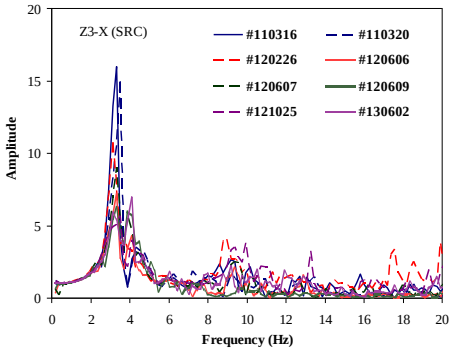

(a) Longitudinal

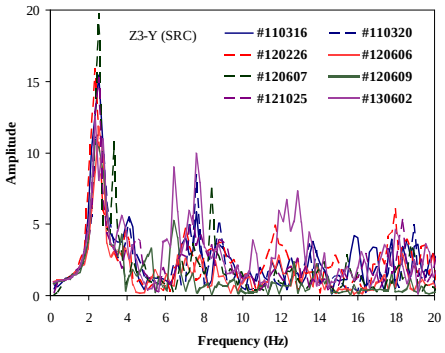

(b) Transverse

Fig. 13 Transfer functions at the Z3 axis

Figs. 11(b), 12(b), and 13(b). The transfer functions reveal that both the RC and SRC frames had approximate fundamental periods in the longitudinal and transverse directions. Furthermore, some studies indicated that the

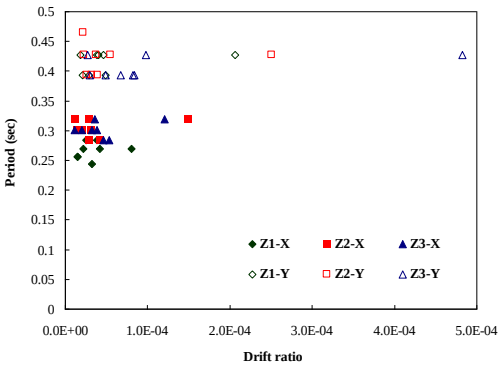

Fig. 14 Variation of period with the peak roof drift ratio

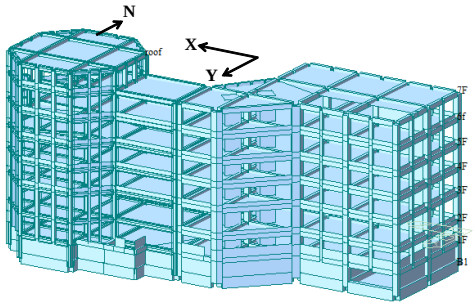

Fig. 15 A global view of the structural model

vibration period may be dependent on the intensity of ground motions (Clinton *et al*. 2006). Fig. 14 shows the variation of the estimated periods with the drift ratios under the eight ground motions. It is seen that the drift ratio had minor influence on the natural period of the department building. All the estimated periods were lower than the design period (0.77 sec) obtained from the code formula. This is probably caused by the many exterior and interior non-structural infills in the building. Those infills can significant increase the lateral structural stiffness under small ground motions. An average period of 0.28 sec was obtained for the Z1 axis and 0.32 sec for the Z2 and Z3 axes in the longitudinal direction. The average period was 0.42 sec for all three vertical axes in the transverse direction.

5. Time-history simulation

A finite element model of the fire department building was constructed with the MIDAS-GEN commercial program (MIDAS 1989) in this study. All the frame members of the RC and SRC frames were modeled as beam-column elements. Thick plate elements were used to simulate the RC slabs, core walls of elevators, and external retaining walls. They were also used in the simulation of interior brick partitions and exterior one meter-high squat walls with a different elastic modulus. Fig. 15 shows a global view of the structural model. Pinned boundary conditions were assumed for the RC raft foundations. The RC retaining walls is 20 cm thick in the south and east façades and 30 cm thick in the north and west façades. The thickness of the RC slabs is 15 cm. The design compressive strength of concrete is 27.5 MPa (280 kgf/cm^2). There are

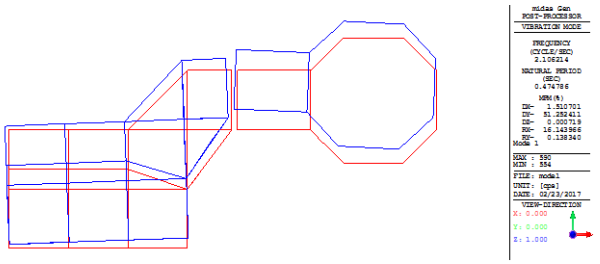

Fig. 16(a) Top view of the 1st modal shape

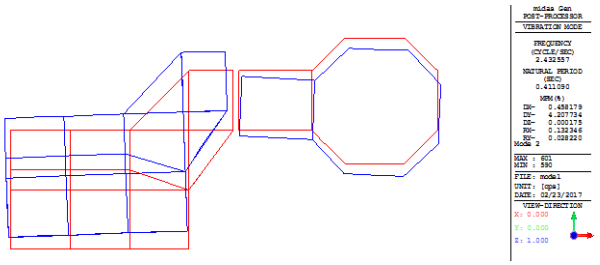

Fig. 16(b) Top view of the 2nd modal shape

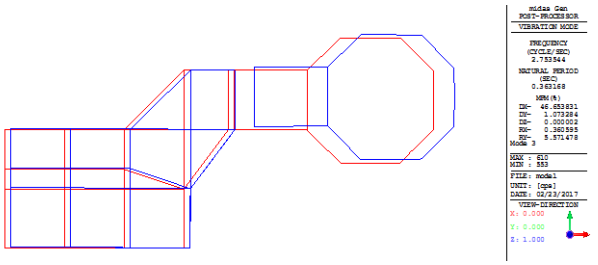

Fig. 16(c) Top view of the 3rd modal shape

around ten different section dimensions each for the beams and columns. In addition to extremely deep section for the B1F beams, most beams and columns of the RC frame were designed with section dimensions of 55×80 cm^2 and 90×90 cm^2, respectively. Most SRC beams were designed with H-sections varying from H-450×200 to H-900×300 made of A36 material and enclosed by 55×80 cm^2 RC sections. Also, most SRC columns were designed with 2H-500×300 and □-500×500 made of A572-50 material and enclosed by 80×80 cm^2 RC sections.

A fundamental period of 0.47 and 0.36 sec in the transverse and longitudinal direction, respectively, were obtained from the eigenvalue analysis of the numerical structural element model. The first structural mode was involved with transverse translation and rotation, as shown in Fig. 16(a). The second one had a modal period of 0.41 sec in transverse translation but with less rotation, as shown in Fig. 16(b). The first longitudinal translation mode turned out to be the third structural mode, as shown in Fig. 16(c). The periods of the structural model were approximately 12% larger than that estimated from the transfer functions. In fact, even as fixed boundary conditions were imposed at the ground level, only a slight change in the periods was obtained for the structural model. This implies that the retaining walls below the ground level behaved as a rigid body under the earthquake, which is consistent with the previous observation in Figs. 7, 8, and 9. Since the finite element model had included all the structural and non-structural walls of the department building, it was regarded as truly realistic and thus used in the following time-history simulations.

Time-history simulations of the structural model under the 2012/02/26 earthquake were carried out with direct integration method. In order to capture the most accurate seismic response, individual time history analyses with mass-proportional damping for each horizontal direction of the three vertical axes (Z1, Z2, and Z3) were conducted at first. The acceleration time histories of the 7F were compared with the measured response. Hence, there were six individual single-directional simulations in total. Afterwards, the damping ratios determined from the single-directional simulations were used to construct the Rayleigh damping models for bi-directional simulations of the seismic response at the three vertical axes. There were three bi-directional simulations at this stage. The analysis results of this stage could be used to evaluate the influence of torsional behavior on the seismic response. At last, the average damping ratios obtained from the individual time-history simulations were used to construct the Rayleigh damping model (Chopra 1995) for the RC and SRC compound building structure. This attempt was intended to evaluate the validity of seismic response simulation of the department building using a single compound structural model.

5.1 Single-directional simulations with mass-proportional damping

A trial damping ratio was used for the first single-directional simulation. Then, the damping ratio was adjusted to reach better consistency between the simulated and measured acceleration time histories. The error index for evaluating the fitness between the measured and simulated time histories was calculated as

$$ERR = \frac{\sqrt{\sum_{i=1}^{N} (A_{p,i} - A_{r,i})^2 / N}}{A_{r,\,peak}} \tag{2}$$

where $A_{p,i}$ and $A_{r,i}$ are respectively the i-th step of the simulated and measured acceleration time histories. N is the number of total points and $A_{r,peak}$ is the peak acceleration of the measured response. The error index was calculated for the 7F acceleration time histories. Another trial time-history analysis was conducted with a different damping ratio to determine the decreasing trend of the error index. Thereafter, the damping ratio was varied for each time-history analysis until the decreasing trend of the error index reversed. Since the damping ratio was obtained from the simulation of the 7F acceleration time histories, it might not minimize the difference between the recorded and predicted time histories for other locations.

The simulated and measured acceleration time histories of the 7F at the Z1, Z2, and Z3 location are compared in Figs. 17(a), 17(b), and 17(c), respectively, and good consistency can be observed from the figures. The obtained damping ratio for best-fit time-history simulation is shown in each figure. Approximate floor acceleration envelopes

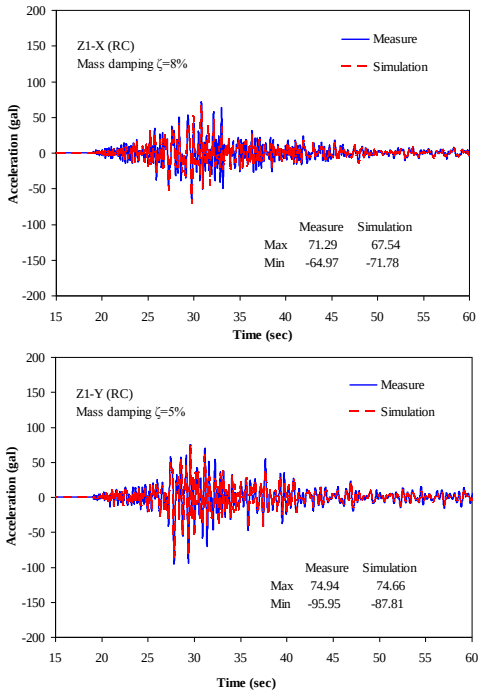

Fig. 17(a) Acceleration time-history simulation at the Z1 location

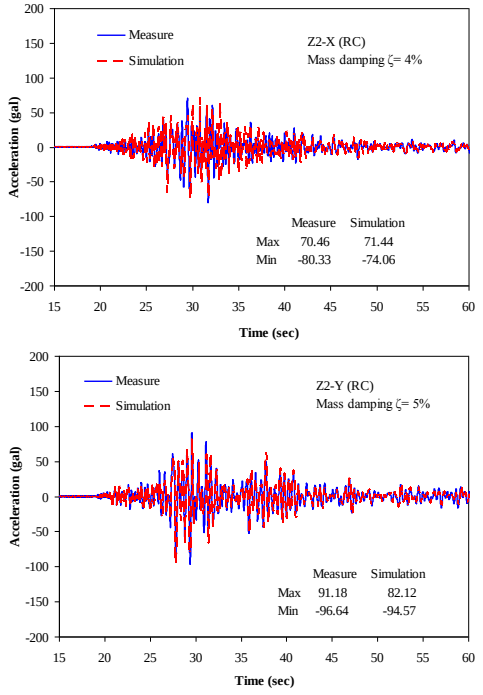

Fig. 17(b) Acceleration time-history simulation at the Z2 location

were also obtained at the Z1, Z2, and Z3 axes, which are not shown here. The numerical results reveal that different damping ratios may be required to have accurate simulations of structural response at different locations.

5.2 Bi-directional simulations with Rayleigh damping

In this section, the numerical structural response of the

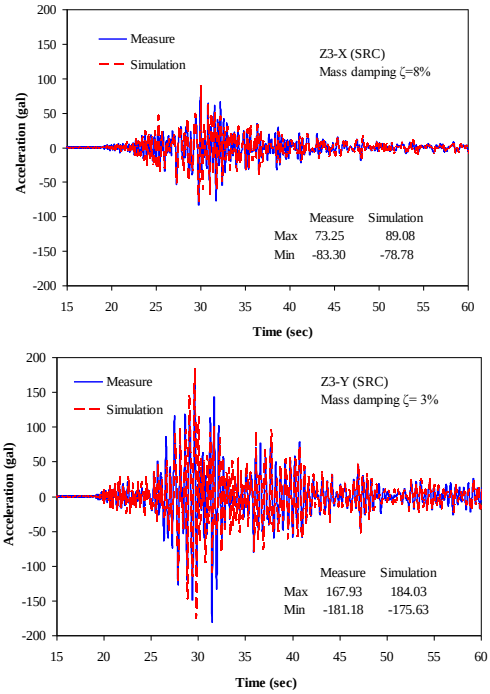

Fig. 17(c) Acceleration time-history simulation at the Z3 location

fire department building under the bi-directional seismic excitations is examined with the damping ratios determined from the single-directional simulations. Rayleigh damping models at the Z1, Z2, and Z3 axis were constructed with the best-fit longitudinal and transverse damping ratios determined in the previous section. The Rayleigh damping coefficients were calculated as

$$\alpha = \frac{2(\xi_Y \omega_X - \xi_X \omega_Y)}{(\omega_X^2 - \omega_Y^2)} \omega_Y \omega_X \tag{3}$$

$$\beta = \frac{2(\xi_X \omega_X - \xi_Y \omega_Y)}{(\omega_X^2 - \omega_Y^2)} \tag{4}$$

where ξ_Y, ω_Y, ξ_X, and ω_X were respectively the damping ratio and fundamental frequency in the transverse (Y) and the longitudinal (X) direction. The constant α and β correspond to the mass and stiffness proportional damping coefficient, respectively. They were used to construct the matrix of damping constants in the time-history analysis. Therefore, the structural responses at the three locations were obtained with three individual bi-directional time-history simulations. Figs. 18(a), 18(b), and 18(c) show the comparisons of the floor acceleration envelopes at the Z1, Z2, and Z3 axes, respectively. It is seen that both the measured and simulated acceleration envelopes were in satisfactory agreement. This implies that orthogonal effect on the structural response was insignificant for the fire department building. Nevertheless, more error is observed for the SRC frame. More significant torsional vibration could be induced in the SRC frame. Figs. 19(a), 19(b), and 19(c) present the horizontal acceleration orbits of the 7F at the Z1-, Z2-, and Z3-axis locations, respectively. It can be seen that the SRC frame did have more apparent torsional behavior than the RC frame under the earthquake.

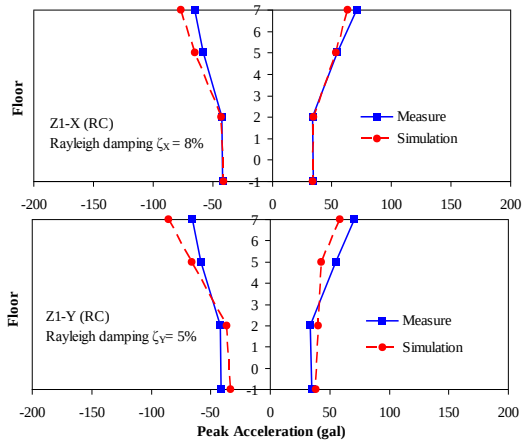

Fig. 18(a) Bi-directional floor acceleration envelopes at Z1 location

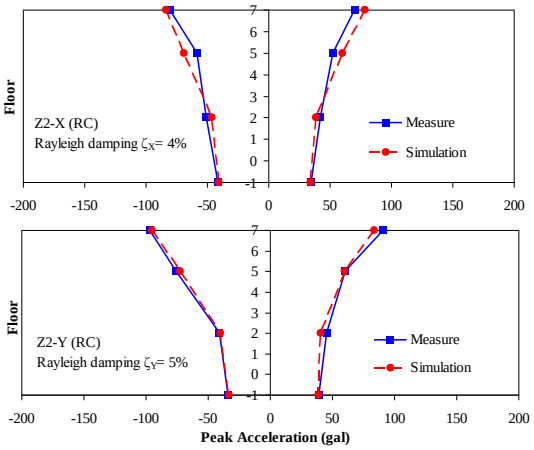

Fig. 18(b) Bi-directional floor acceleration envelopes at Z2 location

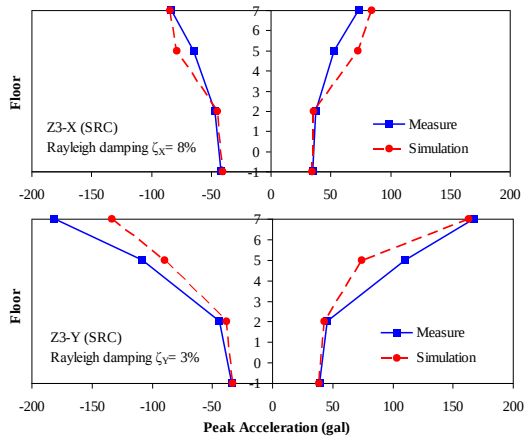

Fig. 18(c) Bi-directional floor acceleration envelopes at Z3 location

Both the single-directional and bi-directional time-history analyses produced good simulation results, even when their damping models induced different damping ratios for higher modes. This suggests that the seismic response of the composite building is primarily governed by the first translational mode in each horizontal direction.

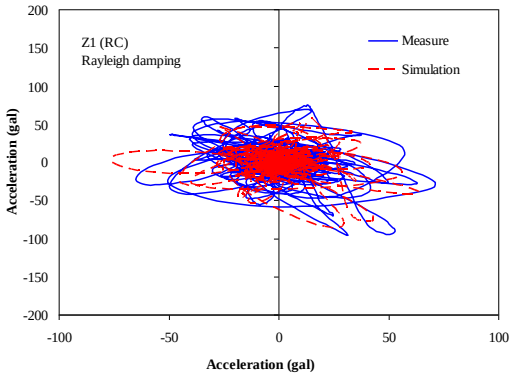

Fig. 19(a) Horizontal acceleration orbits of the 7F at the Z1 location

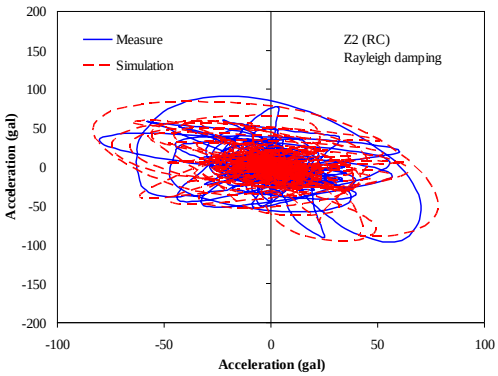

Fig. 19(b) Horizontal acceleration orbits of the 7F at the Z2 location

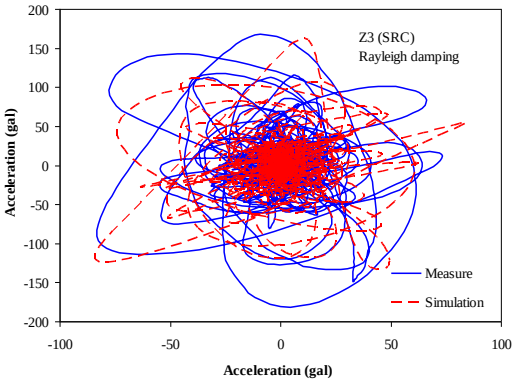

Fig. 19(c) Horizontal acceleration orbits of the 7F at the Z3 location

Consequently, the only damping ratios that mattered were the ones assigned to those modes.

The numerical analyses show that the peak structural response of the fire department building could be captured once the top floor acceleration time histories were accurately simulated. A further attempt was conducted to establish a Rayleigh damping model for the compound RC and SRC building structure with the average damping ratios determined from the Z1, Z2, and Z3 axis. This resulted in a damping ratio of 7% in the longitudinal and 4% in the transverse direction. With this average Rayleigh damping model, the comparisons of the measured and simulated floor acceleration envelopes at the Z1, Z2, and Z3 locations

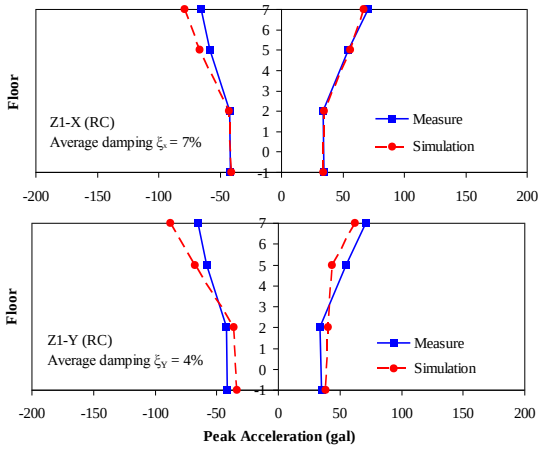

Fig. 20(a) Bi-directional floor acceleration envelopes at Z1 location using average damping ratios

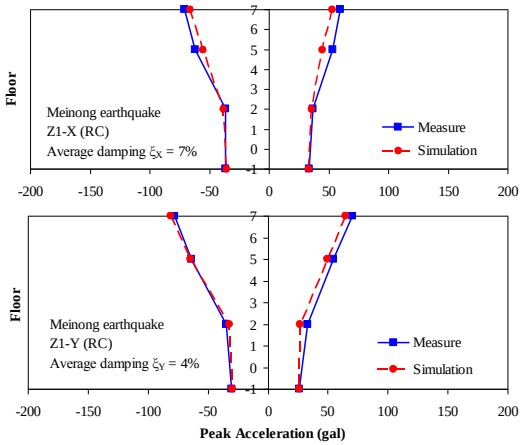

Fig. 21(a) Bi-directional floor acceleration envelopes at Z1 location under Meinong earthquake

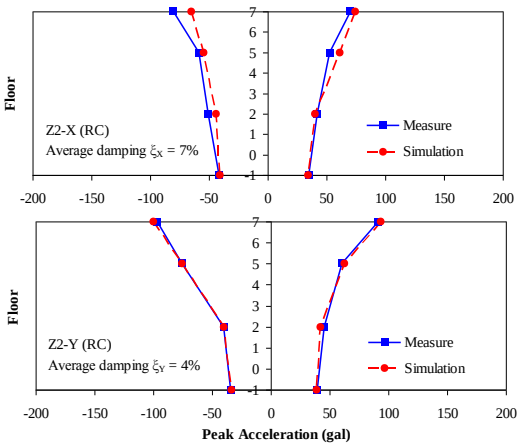

Fig. 20(b) Bi-directional floor acceleration envelopes at Z2 location using average damping ratios

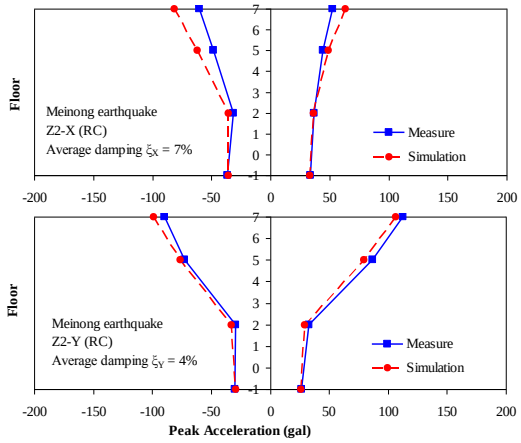

Fig. 21(b) Bi-directional floor acceleration envelopes at Z2 location under Meinong earthquake

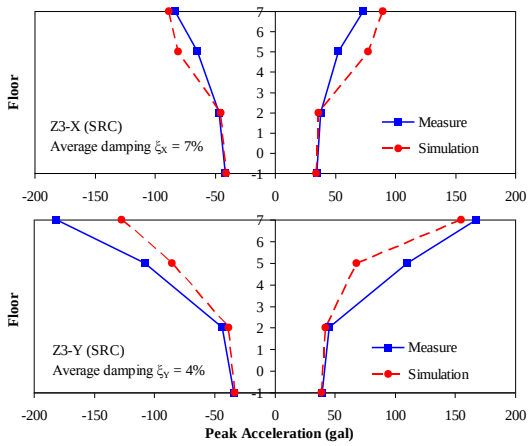

Fig. 20(c) Bi-directional floor acceleration envelopes at Z3 location using average damping ratios

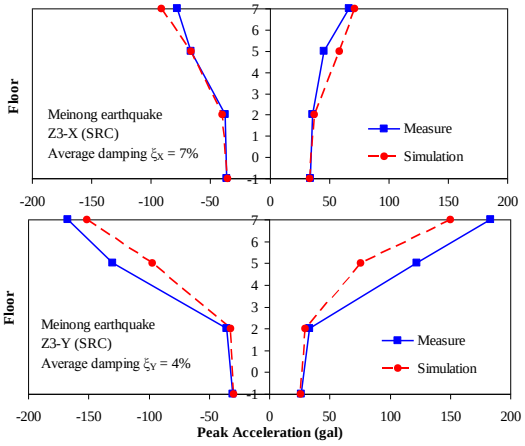

Fig. 21(c) Bi-directional floor acceleration envelopes at Z3 location under Meinong earthquake

are shown in Figs. 20(a), 20(b), and 20(c), respectively. It can be observed that approximate peak accelerations could be obtained with the compound structural model, although the accuracy was not as good as the individual simulation results.

In order to provide more validation for the structural model, bi-directional time-history simulation for the seismic response of the fire department building under the Meinong earthquake on February 6, 2016, was conducted. The earthquake occurred in Meinong District of Kaohsiung City, Taiwan, and had a Ritcher magnitude of 6.6 (Gilsanz *et al.* 2016). At the site of the fire department building, a free-

field PGA of 42.0 gal and 36.9 gal were respectively recorded in the longitudinal (*X*) and transverse (*Y*) direction of the building plan. With the constructed compound structural model, the predicted peak floor accelerations are compared with the measured ones at the Z1, Z2, and Z3 locations, as shown in Figs. 21(a), 21(b), and 21(c), respectively. It is seen that the structural model can provide approximate peak acceleration response and hence can be used to simulate the bi-directional seismic response of the fire department building.

6. Conclusions

The Pingtung Fire Department Building located in the southernmost county of Taiwan was built in 2000 and instrumented with thirty-two accelerometers for seismic response observation in 2010. The building is composed of an RC and an SRC structural frame. Both frames shares a common basement and are separated with an expansion joint from the first to the seventh floor. The accelerometers were deployed at the B1F, 2F, 5F, 7F, and RF of the department building. Seismic records of the structural arrays under eight larger earthquakes occurring during the period from 2011 to 2013 have been examined in this study. It was found that the average 5%-damped acceleration response spectrum obtained from the B1F accelerometers is approximate to and enveloped by the seismic design spectrum. This confirms that the design spectrum could adequately reflect the seismic demand of the in-situ ground motions. From the floor acceleration amplifications of the 2F, 5F, and 7F, it was observed that the SRC frame exhibited larger amplification than the RC frame. The empirical formula recommended in the ASCE 7-10 guidelines can generally capture the mean story-wise acceleration amplifications for the building structure except for the transverse response of the SRC frame, which was better enveloped by the empirical formula recommended in UBC-97 design code. Furthermore, an average fundamental period of 0.42 sec and 0.30 sec were obtained from the transfer functions between the 7F and B1F accelerations for the transverse and longitudinal direction, respectively. Both the RC and SRC frames had approximate fundamental periods in either direction. Their periods were slightly changed under the eight earthquakes.

Time-history simulation for the 7F acceleration of the department building under the 2012/02/26 earthquake was carried out. Accurate simulation results were obtained from single-directional time-history analysis with mass-proportional damping for each horizontal direction at the three vertical axis locations. The best-fit damping ratios from the single-directional simulation were used to construct the Rayleigh damping model for bi-directional time-history simulations. From the bi-directional simulation results, it was recognized that the orthogonal effect on the seismic response of the RC and SRC frames was not significant. The seismic response of the composite building was dominated by the first translational mode in each horizontal direction. Therefore, even though the mass-proportional damping and Rayleigh damping models induced different damping ratios for higher modes, they did not significantly affect the simulation results. Also, although spatial variation of structural damping was observed for the department building, approximate floor acceleration envelopes could be obtained with a compound RC and SRC structural model by using the average damping ratios determined from the three different plan locations. However, if the RC and SRC frames exhibited apparently different vibration characteristics, their seismic responses could only be simulated with two separate models.

Acknowledgments

The authors are grateful to the Central Weather Bureau for providing the seismic records and the Pingtung Fire and Emergency Service Bureau for assistance in the field investigation of the department building.

References

Ansari, F. (2005), *Sensing Issues in Civil Structural Health Monitoring*, Springer International Publishing AG, Cham (ZG), Switzerland.

ASCE (2010), Minimum Design Loads for Buildings and Other Structures, Standard ASCE/SEI 7-10, American Society of Civil Engineers, Reston, Virginia.

Bikçe, M. and Çelik, T.B. (2016), "Failure analysis of newly constructed RC buildings designed according to 2007 Turkish Seismic Code during the October 23, 2011 Van earthquake", *Eng. Fail. Anal.*, **64**, 67-84.

Bradford, S.C., Clinton, J.F., Favela, J. and Heaton, T.H. (2004), "Results of Millikan library forced vibration testing", Caltech EERL-2004-03, California Institute of Technology.

Çelebi, M. (2004), "Structural monitoring arrays-past, present and future", *Proceedings of NATO Workshop on Future Directions on Strong Motion and Engineering Seismology*, Kusadasi, Izmir, Turkey, May.

Celebi, M., Sanli, A., Sinclair, M., Gallant, S. and Radulescu, D. (2004), "Real-time seismic monitoring needs of a building owner-and the solution: a cooperative effort", *Earthq. Spectra*, **20**(2), 333-346.

Chopra, A.K. (1995), *Dynamics of Structures: Theory and Applications to Earthquake Engineering*, Prentice-Hall, New Jersey.

Clinton, J.F., Bradford, S.C., Heaton, T.H. and Favela, J. (2006), "The observed wander of the natural frequencies in a structure", *Bull. Seismol. Soc. Am.*, **96**(1), 237-257.

CPA (1997), Seismic Design Code and Commentary for Buildings, Construction and Planning Agency, Ministry of Interior Affair, Taipei, Taiwan. (in Chinese)

Cruz, C. and Miranda, E. (2016), "Evaluation of damping ratios for the seismic analysis of tall buildings", *J. Struct. Eng.*, **143**(1), 04016144-1-10.

Doebling, S.W., Farrar, C.R., Prime, M.B. and Shevitz, D.W. (1996), "Damage identification and health monitoring of structural and mechanical systems from changes in their vibration characteristics: a literature review", Los Alamos National Lab., NM.

FEMA (2003), "NEHRP recommended provisions for seismic regulations for new buildings and other structures", Report No. FEMA 450, Federal Emergency Management Agency, Washington, DC.

Garevski, M. (2013) *Earthquakes and Health Monitoring of Civil Structure*, Springer International Publishing AG, Cham (ZG), Switzerland.

Gilsanz, R., Huang, C., Mandrick, J., Mugford, J., Steficek, C., Çelebi, M. and Jhuang, S.J. (2016), "Learning from the recent Taiwan Meinong earthquake", *Proceedings of the 2016 SEAOC Convention*, Maui, HI, October.

Goel, R.K. and Chopra, A.K. (1998), "Period formulas for concrete shear wall buildings", *J. Struct. Eng.*, **124**(4), 426-433.

ICC (1997), Uniform Building Code, Vol. 2: Structural Engineering Design Provisions, International Code Council, Whittier, CA.

Inel, M. and Meral, E. (2016), "Seismic performance of RC buildings subjected to past earthquakes in Turkey", *Earthq. Struct.*, **11**(3), 483-503.

Irie, Y. and Nakamura, K. (2000), "Dynamic characteristics of a R/C building of five stories based on microtremor measurements and earthquake observations", *Proceedings of the 12th World Conference on Earthquake Engineering (12WCEE)*, Auckland, New Zealand, January-February.

Isik, E. and Kutanis, M. (2015), "Performance based assessment for existing residential buildings in Lake Van basin and seismicity of the region", *Earthq. Struct.*, **9**(4), 893-910.

LATBSDC (2011), An Alternative Procedure for Seismic Analysis and Design of Tall Buildings Located in the Los Angeles Region: A Consensus Document, Los Angeles Tall Buildings Structural Design Council.

Lemnitzer, A., Massone, L.M., Skolnik, D.A., de la Llera Martin, J.C. and Wallace, J.W. (2014), "Aftershock response of RC buildings in Santiago, Chile, succeeding the magnitude 8.8 Maule earthquake", *Eng. Struct.*, **76**, 324-338.

Michel, C., Guéguen, P., Arem, S.E., Mazars, J. and Kotronis, P. (2010), "Full-scale dynamic response of an RC building under weak seismic motions using earthquake recordings, ambient vibrations and modeling", *Earthq. Eng. Struct. Dyn.*, **39**, 419-441.

MIDAS (1989), Integrated Solution System for Building and General Structures, MIDAS Information Technology Co., Livonia, MI 48152, USA.

Mihailov, V., Celebi, M. and Talaganov, K. (2000), "Seismic monitoring of structures-an important element of seismic hazard reduction", *Proceeding of the 12th World Conference of Earthquake Engineering (12WCEE)*, Auckland, New Zealand, January-February.

Mucciarelli, M., Masi, A., Gallipoli, M.R., Harabaglia, P., Vona, M., Ponzo, F. and Dolce, M. (2004), "Analysis of RC building dynamic response and soil-building resonance based on data recorded during a damaging earthquake (Molise, Italy, 2002)", *Bull. Seismol. Soc. Am.*, **94**(5), 1943–1953.

Ruiz-Pinilla, J.G., Adam, J.M., Pérez-Cárcel, R., Yusteb, J. and Moraguesa, J.J. (2016), "Learning from RC building structures damaged by the earthquake in Lorca, Spain, in 2011", *Eng. Fail. Anal.*, **68**, 76-86.

Sharma, K., Deng, L. and Noguez, C.C. (2016) "Field investigation on the performance of building structures during the April 25, 2015, Gorkha earthquake in Nepal", *Eng. Struct.*, **121**, 61-74.

Shin, T.C., Tsai, Y.B., Yeh, Y.T., Liu, C.C. and Wu, Y.M. (2002), "Strong-motion instrumentation programs in Taiwan", *Int. Handbook Earthq. Eng. Seismol.*, **81B**, 1057-1062.

Skolnik, D., Lei, Y., Yu, E. and Wallace, J.W. (2006), "Identification, model updating, and response prediction of an instrumented 15-story steel-frame building", *Earthq. Spectra*, **22**(3), 781-802.

Takewaki, I., Fujita, K. and Yoshitomi, S. (2013), "Uncertainties in long-period ground motion and its impact on building structural design: Case study of the 2011 Tohoku (Japan) earthquake", *Eng. Struct.*, **49**, 119-134.

Ventura, C.E., Liam Finn, W.D., Lord, J.F. and Fujita, N. (2003), "Dynamic characteristics of a base isolated building from ambient vibration measurements and low level earthquake shaking", *Soil Dyn. Earthq. Eng.*, **23**, 313-322.

Yu, E., Skolnik, D., Whang, D.H. and Wallace, J.W. (2008), "Forced vibration testing of a four-story reinforced concrete building utilizing the nees@UCLA mobile field laboratory", *Earthq. Spectra*, **24**(4), 969-995.

CC